Dynamic Modeling and Nonlinear Model Predictive Control of a Moving Bed Chemical Looping Combustion Reactor

Robert B. Parker * **Lorenz T. Biegler** **

* *Carnegie Mellon University, Pittsburgh, PA 15232 USA (e-mail: rparker1@andrew.cmu.edu).*
** *Carnegie Mellon University, Pittsburgh, PA 15232 USA (e-mail: biegler@cmu.edu)*

Abstract: A partial differential-algebraic equation (PDAE) model of a dynamic moving bed chemical looping combustion reduction reactor is developed in the IDAES process modeling framework for nonlinear model predictive control (NMPC). Numerical stability of the PDAE discretization and the index-1 property of the DAE are validated. An NMPC case study is performed, which manipulates inlet flow rates to control the system to a steady-state setpoint over approximately 6,000 s of simulated time, while respecting a lower bound on outlet oxygen carrier conversion. The dynamic optimization problems are solved for each NMPC cycle with an average of 39 CPUs, indicating that this model has the potential for use in a real-time scenario.

Keywords: Modeling, Optimization, Nonlinear control, Reactor control, Partial differential equations

1. INTRODUCTION

To meet increasing global energy demands while reducing carbon dioxide emissions, there is a need for advanced combustion technologies that are conducive to carbon capture, either through post-combustion absorption or through isolation of carbon dioxide from nitrogen. One such technology is chemical looping combustion, in which a gaseous hydrocarbon fuel reduces a solid oxygen carrier in one reactor and air oxidizes the oxygen carrier in another (Fan (2010)). The oxygen carrier is repeatedly oxidized and reduced by looping between the air and fuel reactor beds, respectively. Because air never comes into contact with the hydrocarbon fuel, the carbon dioxide-water vapor product from the fuel (i.e., reduction) reactor can be easily separated for carbon capture and storage. As this technology has not been implemented widely at large scale, there is a need for simulations that capture the physics, dynamics, and chemistry of the process at operating conditions of interest. These operating conditions may be dynamic due to time-varying prices and demands.

Simultaneous, equation-oriented dynamic models are attractive for their versatility and amenability to many different optimization studies, including nonlinear model predictive control (NMPC). Several authors have studied dynamic equation-oriented chemical looping combustion models. Noorman et al. (2011) perform dynamic simulation studies on a three-stage chemical looping combustion cycle (oxidation, reduction, purge) in a fixed bed reactor and Han and Bollas (2016) perform dynamic optimization studies on the same cycle, although they restrict input variables to have constant values over each stage. With a similar process, Lucio and Ricardez-Sandoval (2020) perform dynamic optimization with time-varying input trajectories and Toffolo and Ricardez-Sandoval (2021) perform simultaneous optimization of design and operation.

While optimization studies with equation-oriented dynamic models have been reported in the literature, these models can be difficult to converge. Details provided by previous dynamic chemical looping case studies suggest that this is the case. Noorman et al. (2011) use extremely small timesteps (approximately 1 ms) in their simulations due to limits of numerical stability, and Lucio and Ricardez-Sandoval (2020) report solve times of over 1,200 CPU s for a simultaneous dynamic optimization formulation, which is too long for a real-time implementation. Han and Bollas (2016) solve the dynamic optimization problem with a sequential dynamic optimization method and do not report solve times. Because of potential difficulties in formulating a tractable dynamic optimization problem, validation of assumptions for the model and controller design is an essential step in the process of evaluating a case study with a dynamic model.

The contributions of this work are the development of a partial differential-algebraic equation (PDAE) model of a chemical looping combustion reduction reactor operating in a moving-bed regime, an NMPC study that achieves a setpoint transition while respecting a bound on outlet conversion, and validation of two important properties of the model: the numerical stability of the PDAE discretization and the index-1 property of the spatially discretized differential-algebraic equation (DAE) model. The code used to produce these results may be found at `github.com/idaes/publications`.

2. MOVING BED CLC REACTOR MODEL

We model a chemical looping combustion reduction reactor in which methane reacts with an iron oxide oxygen carrier on an aluminum oxide support to produce carbon dioxide and steam. The reduction reaction in this process is

$$\mathrm{CH_4} + 12\mathrm{Fe_2O_3} \rightarrow 2\mathrm{H_2O} + \mathrm{CO_2} + 8\mathrm{Fe_3O_4}, \quad (1)$$

and the reactor is assumed to operate in a moving bed regime. We assume that the contents of the reactor are radially well-mixed, axial diffusion may be ignored, the solid phase moves with a uniform velocity, an Ergun equation is sufficient to calculate pressure change, and the gas phase behaves like an ideal gas. Degrees of freedom are inlet flow rates, temperatures, compositions, and gas phase pressure. Inlet flow rates are manipulated inputs, while other inputs may be treated as disturbances. Nominal inlet operating conditions are a gas flow rate of 128 mol/s, a solid flow rate of 591 kg/s, a gas temperature of 298 K, a solid temperature of 1,183 K, a gas composition of 97.5% $\mathrm{CH_4}$ and 2.5% $\mathrm{CO_2}$ by mole, a solid composition of 45% $\mathrm{Fe_2O_3}$ and 55% $\mathrm{Al_2O_3}$ by mass, and a pressure of 2.0 bar. This process has been modeled at steady state in a previous study by Okoli et al. (2020).

2.1 PDAE Model

The process is modeled as a system of nonlinear partial differential-algebraic equations (PDAE). Our assumptions lead to a system with differential equations in time t and along the normalized length of the reactor z. The differential equations are the gas phase mass balances (2), the gas phase energy balance (3), the solid phase mass balances (4), the solid phase energy balance (5), and the Ergun equation (6).

$$l\frac{\partial M_i}{\partial t} = \frac{\partial f_i}{\partial z} + lN_{i,g}\ , \quad i \in \{\mathrm{CH_4}, \mathrm{CO_2}, \mathrm{H_2O}\} \quad (2)$$

$$l\frac{\partial H_g}{\partial t} = \frac{\partial f_{H,g}}{\partial z} + lQ_g \quad (3)$$

$$l\frac{\partial M_i}{\partial t} = \frac{\partial f_i}{\partial z} + lN_{i,s}\mathrm{MW}_i\ , \quad i \in \{\mathrm{Fe_2O_3}, \mathrm{Fe_3O_4}, \mathrm{Al_2O_3}\} \quad (4)$$

$$l\frac{\partial H_s}{\partial t} = \frac{\partial f_{H,s}}{\partial z} - lQ_g + \Delta H_{\mathrm{rxn}}\xi \quad (5)$$

$$\frac{\partial P}{\partial z} = 150\frac{(1-\epsilon)^2\mu(v_g+v_s)}{d_p^2\epsilon^3} + \frac{7}{4}\frac{\rho_{g,\mathrm{mass}}(1-\epsilon)(v_g+v_s)^2}{d_p\epsilon^3} \quad (6)$$

In these equations, $l = 5$ m is the length of the reactor, M_i is the material holdup of species i, f_i is the flow rate of i, $N_{i,g}$ is the rate of transport of i into the gas phase, $N_{i,s}$ is the rate of transport of i into the solid phase, MW_i is the molecular weight of i, H_g is the gas phase enthalpy holdup, H_s is the solid phase enthalpy holdup, $f_{H,g}$ is the gas phase enthalpy flow rate, $f_{H,s}$ is the solid phase enthalpy flow rate, Q_g is the rate of heat transfer into the gas phase, ΔH_{rxn} is the enthalpy of reaction (1), ξ is the extent of reaction (1), P is pressure, ϵ is the bed void fraction, μ is kinematic viscosity, v_g is gas phase velocity, v_s is solid phase velocity, $\rho_{g,\mathrm{mass}}$ is gas phase mass density, and $d_p = 1.5$ mm is the particle diameter.

Initial conditions are provided in terms of material and enthalpy holdups and consist of a profile of these variables along the length of the reactor. Boundary conditions relating to inlet flow rates, temperatures, mole fractions, and pressure are imposed at every point in time. Algebraic equations calculate reaction rate, thermodynamic properties, and rates of mass and heat transfer. Selected algebraic equations that are relevant for the index analysis of Section 4 are the Nusselt number equation (7), the Shomate equations (8) and (9), the enthalpy mixture equations (10) and (11), the density equations (12) and (13), and the summation equations (14) and (15).

$$\mathrm{Nu}_p^3 = \left(2 + 1.1\mathrm{Re}_p^{1.8}\right)\mathrm{Pr} \quad (7)$$

$$\hat{H}_{g,i} = A_{H,i}T_g + B_{H,i}T_g^2 + C_{H,i}T_g^3 + D_{H,i}T_g^4 + \frac{E_{H,i}}{T_g} + F_{H,i}\ , \quad i \in \{\mathrm{CH_4}, \mathrm{CO_2}, \mathrm{H_2O}\} \quad (8)$$

$$\hat{H}_{s,i} = A_{H,i}T_s + B_{H,i}T_s^2 + C_{H,i}T_s^3 + D_{H,i}T_s^4 + \frac{E_{H,i}}{T_s} + F_{H,i}\ , \quad i \in \{\mathrm{Fe_2O_3}, \mathrm{Fe_3O_4}, \mathrm{Al_2O_3}\} \quad (9)$$

$$\hat{H}_g = \sum_{i\in\{\mathrm{CH_4},\mathrm{CO_2},\mathrm{H_2O}\}} y_i H_{g,i} \quad (10)$$

$$\hat{H}_s = \sum_{i\in\{\mathrm{Fe_2O_3},\mathrm{Fe_3O_4},\mathrm{Al_2O_3}\}} x_i H_{s,i} \quad (11)$$

$$\rho_i = y_i\rho_g\ , \quad i \in \{\mathrm{CH_4}, \mathrm{CO_2}, \mathrm{H_2O}\} \quad (12)$$

$$\rho_i = x_i\rho_s\ , \quad i \in \{\mathrm{Fe_2O_3}, \mathrm{Fe_3O_4}, \mathrm{Al_2O_3}\} \quad (13)$$

$$\sum_{i\in\{\mathrm{CH_4},\mathrm{CO_2},\mathrm{H_2O}\}} y_i = 1 \quad (14)$$

$$\sum_{i\in\{\mathrm{Fe_2O_3},\mathrm{Fe_3O_4},\mathrm{Al_2O_3}\}} x_i = 1 \quad (15)$$

where Nu_p is the particle Nusselt number, Re_p is the particle Reynolds number, Pr is the Prandtl number, $\hat{H}_{g,i}$ is the specific enthalpy of species i, $A_{H,i} \ldots F_{H,i}$ are the Shomate equation coefficients for species i, $\hat{H}_g$ is the gas phase specific enthalpy, $\hat{H}_s$ is the solid phase specific enthalpy, ρ_i is the density of species i, y_i is the gas phase mole fraction of species i, x_i is the solid phase mass fraction of species i, ρ_g is the total gas phase density, and ρ_s is the total solid phase density. Additional important algebraic variables are the solid conversion X_{OC}, the fraction of iron in the oxygen carrier that is reduced, and the reaction rate r_{rxn}. These are calculated by Equations (16) and (17).

$$X_{\mathrm{OC}} = \frac{x_{\mathrm{Fe_3O_4}}}{x_{\mathrm{Fe_3O_4}} + \frac{2\mathrm{MW}_{\mathrm{Fe_3O_4}}}{3\mathrm{MW}_{\mathrm{Fe_2O_3}}}x_{\mathrm{Fe_2O_3}}} \quad (16)$$

$$r_{\mathrm{rxn}} = 3\frac{a_{\mathrm{vol}}}{r_p}k_{\mathrm{rxn}}x_{\mathrm{Fe_2O_3,mol}}\rho_{\mathrm{CH_4}}^{1.3}\left(1 - X_{\mathrm{OC}}\right)^{2/3} \quad (17)$$

Here, r_p is the particle radius, a_{vol} is the fraction of particle volume available for reaction, k_{rxn} is a reaction coefficient defined by an Arrhenius rule, and $x_{\mathrm{Fe_2O_3,mol}}$ is the mole fraction of $\mathrm{Fe_2O_3}$ in the particle. This reaction rate is given by Abad et al. (2007) and assumes that diffusion through the particle grain is the dominating resistance to mass transfer. Further reduction of $\mathrm{Fe_3O_4}$ to FeO and Fe may occur, but we defer modeling of this more complicated reaction sequence to future work. It is desirable to maintain a high oxygen carrier conversion so the subsequent exothermic oxidation reaction produces the maximum amount of thermal energy per unit of oxygen carrier cycled.

The model is implemented using the IDAES process modeling framework (Lee et al. (2021)). IDAES is a process modeling framework built on top of the Pyomo (Bynum et al. (2021)) algebraic modeling environment that provides a streamlined interface for constructing chemical process models in optimization-ready algebraic systems. The full set of algebraic equations for the PDAE model, as well as the values of all parameters used, may be accessed via IDAES repository at `github.com/idaes/idaes-pse`.

2.2 Spatially discretized DAE model

To use our PDAE model in a nonlinear model predictive control (NMPC) study, we first convert our system into an initial value problem. To do this, we discretize the spatial domain, leaving us with a system of differential and algebraic equations (DAE) subject to initial conditions. The DAE representing our system after spatial discretization has the form given by the following DAE and initial condition:

$$\left.\frac{da}{dt}\right|_t = f(a_t, b_t, u_t), \quad a_0 = \bar{a}_0 \tag{18a}$$

$$0 = g(a_t, b_t, u_t)\ , \tag{18b}$$

where a is the vector of time-differential variables, b is the vector of algebraic variables, and u is the vector of manipulated inputs. The differential equations are the reactor mass and energy balances and algebraic equations are all other equations, including the Ergun equation, which contains a spatial derivative but no time derivative.

Motivated by countercurrent flow, we choose an upwind derivative discretization in the spatial domain, with gas phase flows (q^g) in the positive direction and the solid phase flows (q^s) in the negative direction, as shown by Equation (19a) and Equation (19b), respectively.

$$\left.\frac{\partial q^g}{\partial z}\right|_{z_i} = \frac{1}{\Delta z}\left(q^g_{z_i} - q^g_{z_{i-1}}\right) \tag{19a}$$

$$\left.\frac{\partial q^s}{\partial z}\right|_{z_i} = \frac{1}{\Delta z}\left(q^s_{z_{i+1}} - q^s_{z_i}\right) \tag{19b}$$

We also note that this discretization is different from the backward discretization used for both solid and gas phase states in Okoli et al. (2020).

2.3 Fully discretized model

Our approach to model predictive control uses the fully discretized formulation of Cuthrell and Biegler (1987). We solve the finite horizon optimal control problem as a nonlinear program (NLP) with the dynamic model represented by a system of nonlinear algebraic equations, derived from an implicit Euler discretization of the DAE system (18). Moreover, because of the index-1 property, Equation (18b) and the algebraic states can be implicitly eliminated to form an ODE. Temporal implicit Euler discretization of this ODE then leads to the concise representation of Equation (20).

$$\begin{aligned} a_{t_{i+1}} &= \bar{f}(a_{t_i}, u_{t_i}) \text{ for all } i \neq 0 \\ a_0 &= \bar{a}_0 \end{aligned} \tag{20}$$

The PDAE system thus becomes a system of nonlinear equality constraints in an optimization problem sent to a standard NLP solver.

3. DISCRETIZATION STABILITY

Because this PDAE model has not been used in a previous simulation or optimization case study, we need to ensure that our chosen time and space discretization is stable in the sense that solutions satisfying the discretized PDAE converge as the discretization grid is refined. Discretization stability is necessary for our algebraic model to accurately approximate the continuous time and space system it is based on. For a linear PDE describing countercurrent flow, stability of an upwind discretization is well established (LeVeque (2002)). In contrast, our discretized moving bed model is nonlinear and also contains the Ergun equation with a spatial derivative but no time derivative. Since we are not aware of a general stability result for our PDAE model, we demonstrate stability for a particular simulation that represents a range of operating conditions of interest. The simulation begins with the model at its nominal steady state and considers a perturbation in inlet gas flow rate from 97.5% methane to 50% methane. The inlet flow rates start at their nominal values and iterate through every combination of low, medium, and high values for gas and solid flow rates, shifting every 60 s. The values applied are 100, 128, and 200 mol/s for gas flow rate and 500, 591, and 700 kg/s for solid flow rate. The sequence of inlet flow rates applied is shown in Figure 1.

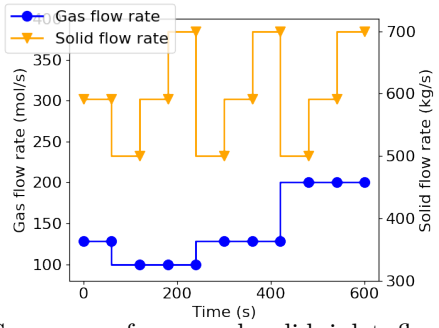

Fig. 1. Sequence of gas and solid inlet flow rates for validation of numerical stability

To verify numerical stability, we simulate the model on a sequence of discretization grids and evaluate approximation errors as the grids are refined. We use a sequence of discretization grids with equally spaced time and space discretization points in which the number of discretization elements increases geometrically, where the i^{th} discretization grid has 2^i discretization elements in the spatial domain and 2^i discretization elements per 60 s of simulation time in the time domain. As the number of discretization points increases, the discretization grid approximates the continuous domain. Here, we simulate the PDAE model for the first seven discretization grids in this sequence. Because our model does not have an analytic solution, we compute error as the difference between simulation solutions on adjacent discretization grids in our sequence. The first six such errors are computed from the first seven discretization grids, and we compute the error for each state variable independently. The chosen state variables (gas and solid total flow rates, mole and mass fractions, temperatures, and pressure) are a subset that is sufficient to calculate all variables in the PDAE model. The computed error for each variable is an approximation of integrated squared error, denoted by ϵ_i in Equation (21), where q_i is one of the PDAE variables above on the i^{th} discretization grid.

$$\epsilon_{q,i} = \int_t \int_z \left(q_{i+1}(t,z) - q_i(t,z)\right)^2 dzdt \tag{21}$$

The difference between q_{i+1} and q_i, solutions for variable q on the $(i+1)^{\text{th}}$ and i^{th} grids, is computed by taking the difference between the variable values at each point in time and space. We approximate this integral using a trapezoidal approximation with the discretization points of the more refined discretization grid. Because the coarser discretization will not have discretization points at all the points of the finer grid, we linearly interpolate the coarse-grid solution onto the more refined grid.

The errors in each variable for the six pairs of discretization grids compared are shown in Figure 2. The results indicate that our PDAE model is stable with the chosen discretization and simulation. This simulation represents a range of operating conditions of interest and justifies our use of the discretized model for simulation and optimization studies.

4. DAE INDEX-1 VERIFICATION

To use the DAE model of Section 2.2 for nonlinear model predictive control, we require the index-1 property to hold. For our semi-explicit DAE, the index-1 property is given by Criterion 1. If a semi-explicit DAE is index-1 according to this criterion, then for fixed differential variables and control inputs, the algebraic equations are always sufficient to solve for the algebraic variables. More information the index of a DAE is given by Ascher and Petzold (1998).

Criterion 1. A semi-explicit DAE is *index-1* if, for all values of differential variables and inputs, the *algebraic Jacobian* (i.e., Jacobian of algebraic equations with respect to algebraic variables) is nonsingular.

Rigorously verifying that a DAE is index-1 requires global analysis that is beyond the scope of this work. Instead, we perform an analysis of the algebraic Jacobian to show under what conditions it becomes singular, then show that it is nonsingular by computing condition numbers over the course of a simulation.

4.1 Structural analysis

To identify conditions under which the algebraic Jacobian matrix may become nonsingular, it is useful to permute it to block triangular form via the approach of Duff and Reid (1978).The sparsity structure of this matrix is shown in Figure 3. This matrix has 785 rows and columns and consists of 665 diagonal blocks as well as a sparse lower triangle. (Rows correspond to equations and columns correspond to variables.) If all diagonal blocks of this matrix are constant and nonsingular, the entire matrix is always nonsingular. In this instance of the DAE model, only 72 out of 665 diagonal blocks are non-constant. These blocks are Jacobians of

(1) Nusselt number equations with respect to Nusselt numbers,
(2) Solid and gas phase enthalpy Shomate equations and enthalpy mixture equations with respect to temperature and component enthalpies,
(3) Solid and gas phase density and sum equations with respect to overall densities and mass/mole fractions,
(4) Ergun equations with respect to gas velocities.

Blocks (1) and (4) each contain a single cubic or quadratic nonlinearity and therefore are nonsingular when their variables do not approach zero. Blocks (3) contain bilinearities and are nonsingular when overall densities do not approach zero and mole/mass fractions do not all approach zero. Only blocks (2) contain general nonlinearities. For the operating conditions of our process, we expect blocks (1), (3), and (4) to be nonsingular at feasible points. While the global analysis of the system in blocks (2) is beyond the scope of this work, the experiment in Section 4.2 suggests that it is nonsingular for many operating points of interest.

4.2 Numerical analysis

To verify that the algebraic Jacobian is nonsingular at a range of feasible operating points, we simulate our DAE following a perturbation from its initial steady state and assemble the algebraic Jacobian at each point in time of the simulation. We permute this Jacobian to block triangular form, and compute the condition number of each diagonal block. Blocks (2) and (3) above have nonlinearities, are larger than 1×1, and are repeated at every spatial discretization point. Figure 4 shows the maximum condition numbers over the spatial discretization for each of these types of blocks at each point in time.

Over this simulation, the nonlinear diagonal blocks of the algebraic Jacobian are nonsingular and have approximately constant condition numbers as shown by Figure 4. This suggests that, near the region encountered by variables in this simulation, the algebraic Jacobian is nonsingular and our DAE model is suitable for NMPC.

5. NONLINEAR MODEL PREDICTIVE CONTROL

Model predictive control is an optimization-based control strategy in which a finite-horizon dynamic optimization problem is solved to calculate a sequence of control inputs, the first of which is sent to the plant. The control input is held constant for one sampling period, after which a measurement from the plant is loaded into the controller in the form of initial condition parameters $\bar{a}_0$, and the control problem is re-solved with this new data (Rawlings et al. (2017)). Points at which measurements are taken and control inputs are applied are referred to as sample points. The NMPC dynamic optimization problem is given by Equation (22), where a^* is a vector of setpoint values for each state variable, and $\mathcal{A}$ and $\mathcal{U}$ are bounds on states and controls. The expression $||a_t - a^*||_2^2$ is referred to as the tracking cost at time t.

$$\begin{aligned} \min_{a,u} & \sum_{i=1}^{N_s} ||a_{t_i} - a^*||_2^2 \\ & a_{t_{i+1}} = \bar{f}(a_{t_i}, u_{t_i}) \text{ for all } t_i \neq 0 \\ & a_0 = \bar{a}_0, a \in \mathcal{A}, u \in \mathcal{U} \end{aligned} \tag{22}$$

In contrast to Equation (20), t now represents a sample point rather than a general time discretization point and i takes values between zero and N_s, the number of samples in a controller horizon.

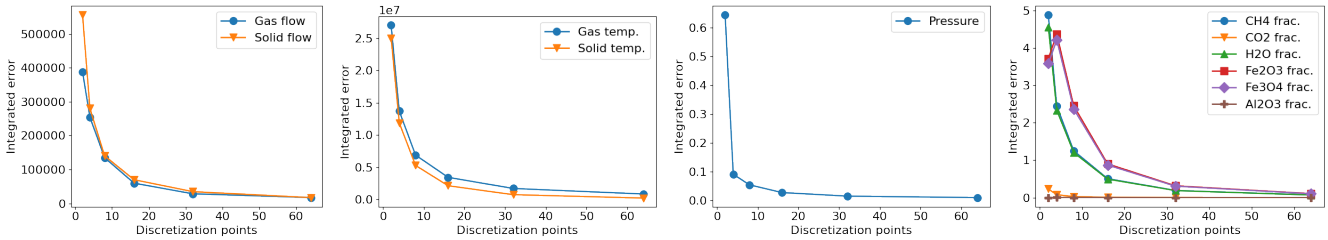

Fig. 2. Discretization error with increasing number of discretization elements. The x-axes contain the number of spatial discretization points and number of temporal discretization points per 60 s, which are the same.

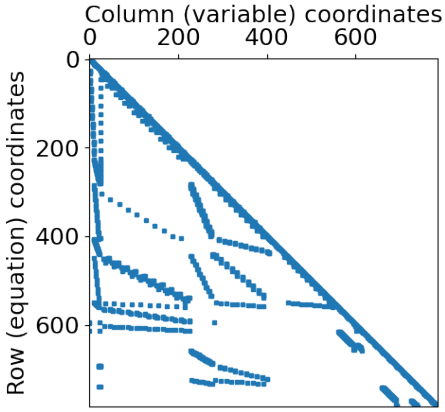

Fig. 3. Sparsity structure of algebraic Jacobian for the DAE model with 10 spatial discretization points

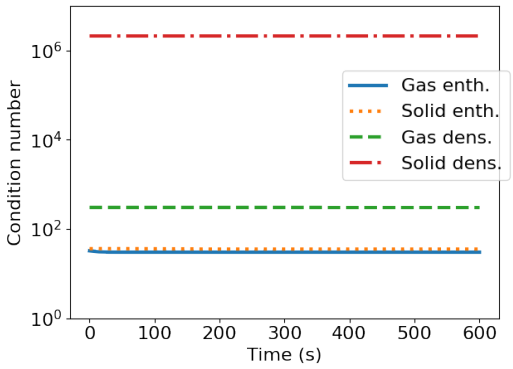

Fig. 4. Maximum diagonal block condition number in each of four categories at each time point

5.1 Control problem

Our control objective is the transition between steady state setpoints induced by a known disturbance to inlet gas composition, and an increase in the outlet solid conversion specification. The initial steady state is that of the nominal operating conditions given in Section 2. The perturbation is a sharp drop in inlet methane concentration from 97.5 % to 50 % and a corresponding increase in inlet CO_2 concentration to 50 %. The outlet conversion of the target steady state is 0.95, compared to 0.90 for the initial steady state. The setpoint values for state variables and inputs are computed by solving a steady state optimization problem with these conditions in which inlet gas flow rate is a degree of freedom that is adjusted to meet the target conversion of 95 %. The gas inlet flow rate needed to meet this target is 273 mol/s.

5.2 NMPC results

The PDE model and Problem (22) is implemented in Pyomo DAE (Nicholson et al. (2018)). The instance used for model predictive control simulation has 10 spatial discretization points, one time discretization point every 60 s, and applies piecewise-constant control action on 180 s intervals. The controller considers ten sampling periods for a horizon of 1,800 s. This discretization spacing is chosen to achieve the relatively fast solve times required for an online application. We initialize the dynamic optimization problem with the results of a previous solve followed by a simulation to ensure a feasible starting point for the optimization. We solve the optimization problem with IPOPT (Wächter and Biegler (2006)). The plant is modeled with the PDAE model presented in this work. The state trajectories from a 6,000 s NMPC simulation are shown in Figure 5, and input trajectories for this NMPC simulation are shown in Figure 6. The optimization problem solved at each sample has 29,623 variables and 29,603 constraints. The plot of tracking cost over time shows a large spike when the setpoint changes and the controller is activated, after 600 s of simulation, then quickly decays to zero as the control action takes effect. This result indicates that our NMPC strategy is sufficient to control this process model to steady state. Tracking cost reaches zero within tolerance after approximately 3,000 s. However, individual states reach their setpoints on very different timescales. Gas phase compositions reach their target steady state values very quickly, in approximately 120 s, while pressure and solid phase compositions do not reach their target steady state values for more than 4,000 s. These results indicate a timescale multiplicity that could be the source of ill-conditioning in our DAE and PDAE models. A faster response in solid phase compositions could be achieved by adjusting weights in the optimization problem (22), but we do not attempt to tune the response in this study.

The outlet solid conversion drops sharply following the decrease in inlet methane composition, but is prevented from violating its lower bound of 0.89 by a sharp increase in inlet gas flow rate and a sharp decrease in inlet solid flow rate that are shown in Figure 6.

In this simulation, the average time spent initializing and solving the dynamic optimization problem is 39 CPU s. However, the longest dynamic optimization problem takes 201 s to initialize and solve. In model predictive control, the dynamic optimization problem is solved online and needs to be completed before the next set of initial conditions from the plant are made available. In this simulation, this means that the optimization problem should be initialized and solved within 180 s. While the average solve time is well within this margin, the maximum

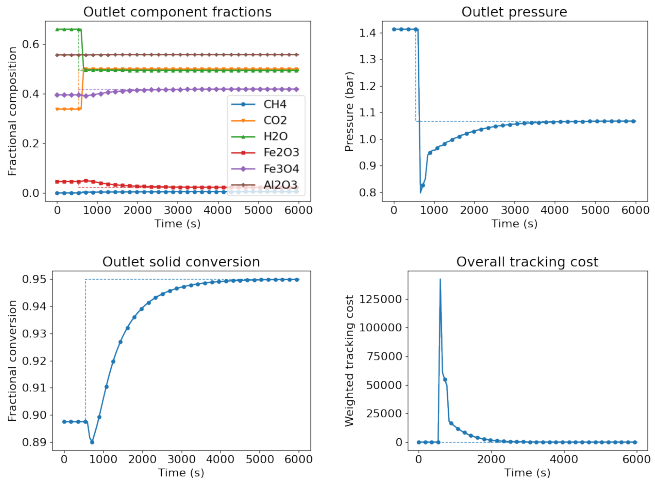

Fig. 5. Selected state trajectories for NMPC simulation over 6,000 s of simulation. Solid lines are plant simulation data, dashed lines are setpoint values. Solid markers indicate sample points.

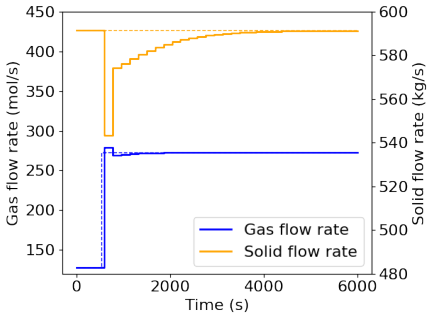

Fig. 6. NMPC input trajectories. Solid lines are applied inputs and dashed lines values at the setpoint.

solve time, which occurs for the first dynamic optimization problem, is slightly too long. Future work will focus on decreasing this dynamic optimization solve time.

6. CONCLUSION

In this work, we have presented a PDAE model of a moving bed chemical looping reduction reactor, validated discretization stability and the DAE index-1 property, and performed an NMPC simulation using the fully discretized PDAE model. Future work will focus on reducing the solve times for the dynamic optimization in our NMPC simulation either via reduced-order modeling strategies or parallel approaches to nonlinear optimization with discretized dynamic systems.

ACKNOWLEDGEMENTS

We gratefully acknowledge Anca Ostace and Chinedu Okoli for help in using the moving bed reactor model.

Disclaimer: This project was funded by the United States Department of Energy, National Energy Technology Laboratory, in part, through a site support contract. Neither the United States Government nor any agency thereof, nor any of their employees, nor the support contractor, nor any of their employees, makes any warranty, express or implied, or assumes any legal liability or responsibility for the accuracy, completeness, or usefulness of any information, apparatus, product, or process disclosed, or represents that its use would not infringe privately owned rights. Reference herein to any specific commercial product, process, or service by trade name, trademark, manufacturer, or otherwise does not necessarily constitute or imply its endorsement, recommendation, or favoring by the United States Government or any agency thereof. The views and opinions of authors expressed herein do not necessarily state or reflect those of the United States Government or any agency thereof.

REFERENCES

Abad, A., Adnez, J., Garca-Labiano, F., de Diego, L.F., Gayn, P., and Celaya, J. (2007). Mapping of the range of operational conditions for Cu-, Fe-, and Ni-based oxygen carriers in chemical-looping combustion. *Chem. Eng. Sci.*, 62(1), 533–549.

Ascher, U.M. and Petzold, L.R. (1998). *Computer methods for ordinary differential equations and differential algebraic equations.*

Bynum, M.L., Hackebeil, G.A., Hart, W.E., Laird, C.D., Nicholson, B.L., Siirola, J.D., Watson, J.P., and Woodruff, D.L. (2021). *Pyomo – Optimization Modeling in Python.* Springer.

Cuthrell, J.E. and Biegler, L.T. (1987). On the optimization of differential-algebraic process systems. *AIChE J.*, 33(8), 1257–1270.

Duff, I.S. and Reid, J.K. (1978). An implementation of Tarjan's algorithm for the block triangularization of a matrix. *ACM Trans. Math. Soft.*, 4, 137–147.

Fan, L.S. (2010). *Chemical Looping Systems for Fossil Energy Conversions.* Wiley.

Han, L. and Bollas, G.M. (2016). Dynamic optimization of fixed bed CLC processes. *Energy*, 112, 1107–1119.

Lee, A., Ghouse, J.H., Eslick, J.C., Laird, C.D., Siirola, J.D., Zamarripa, M.A., Gunter, D., Shinn, J.H., Dowling, A.W., Bhattacharyya, D., Biegler, L.T., Burgard, A.P., and Miller, D.C. (2021). *J. Adv. Manuf. Proc.*, 3(3).

LeVeque, R.J. (2002). *Finite Volume Methods for Hyperbolic Problems.* Cambridge University Press.

Lucio, M. and Ricardez-Sandoval, L.A. (2020). Dynamic modelling and control strategies for CLC in an industrial-scale reactor. *Fuel*, 262.

Nicholson, B.L., Siirola, J.D., Watson, J.P., Zavala, V.M., and Biegler, L.T. (2018). `pyomo.dae`: a modeling and automatic discretization framework for DAE optimization. *Math. Prog. Comp.*, 10, 187–223.

Noorman, S., Gallucci, F., van Sint Annaland, M., and Kuipers, J. (2011). A theoretical investigation of CLC in packed beds. Part 2: Reactor model. *Chem. Eng. J.*, 167, 369–376.

Okoli, C.O., Ostace, A., Nadgouda, S., Lee, A., Tong, A., Burgard, A.P., Bhattacharyya, D., and Miller, D.C. (2020). A framework for the optimization of chemical looping combustion processes. *Powder Tech.*, 149–162.

Rawlings, J.B., Mayne, D.Q., and Diehl, M.M. (2017). *Model Predictive Control Theory, Computation, and Design.* Nob Hill.

Toffolo, K. and Ricardez-Sandoval, L. (2021). Optimal design and control of a multiscale model for a CLC reactor. *IFAC PapersOnLine*, 54(3), 615–620.

Wächter, A. and Biegler, L.T. (2006). On the implementation of an interior-point filter line-search algorithm for large-scale nonlinear programming. *Math. Prog.*, 106, 25–57.